University of Groningen

Different healing characteristics of thiol-bearing molecules on CVD-grown MoS$_2$

Feraco, Giovanna; Luca, Oreste De; Syari'ati, Ali; Hameed, Sardar; El Yumin, Abdurrahman Ali; Ye, Jianting; Agostino, Raffaele G.; Rudolf, Petra

IMPORTANT NOTE: You are advised to consult the publisher's version (publisher's PDF) if you wish to cite from it. Please check the document version below.

Document Version
Publisher's PDF, also known as Version of record

Publication date:
2023

Link to publication in University of Groningen/UMCG research database

PAPER • OPEN ACCESS

Different healing characteristics of thiol-bearing molecules on CVD-grown MoS$_2$

To cite this article: Giovanna Feraco *et al* 2023 *J. Phys. Mater.* **6** 034006

View the article online for updates and enhancements.

Journal of Physics: Materials

PAPER

Different healing characteristics of thiol-bearing molecules on CVD-grown MoS₂

Giovanna Feraco[1] ᴰ, Oreste De Luca[1,4] ᴰ, Ali Syari'ati[1] ᴰ, Sardar Hameed[1,3] ᴰ,
Abdurrahman Ali El Yumin[1] ᴰ, Jianting Ye[1] ᴰ, Raffaele G Agostino[2] ᴰ and Petra Rudolf[1,*] ᴰ

1   Zernike Institute for Advanced Materials, University of Groningen, Nijenborgh 4, 9747AG Groningen, The Netherlands
2   Dipartimento di Fisica, Università della Calabria, 87036 Arcavacata di Rende (Cs), Italy
3   Department of Physics, University of Malakand, Khyber Pukhtoonkhwa, Pakistan
4   Present address: Dipartimento di Fisica, Università della Calabria, 87036 Arcavacata di Rende (Cs), Italy
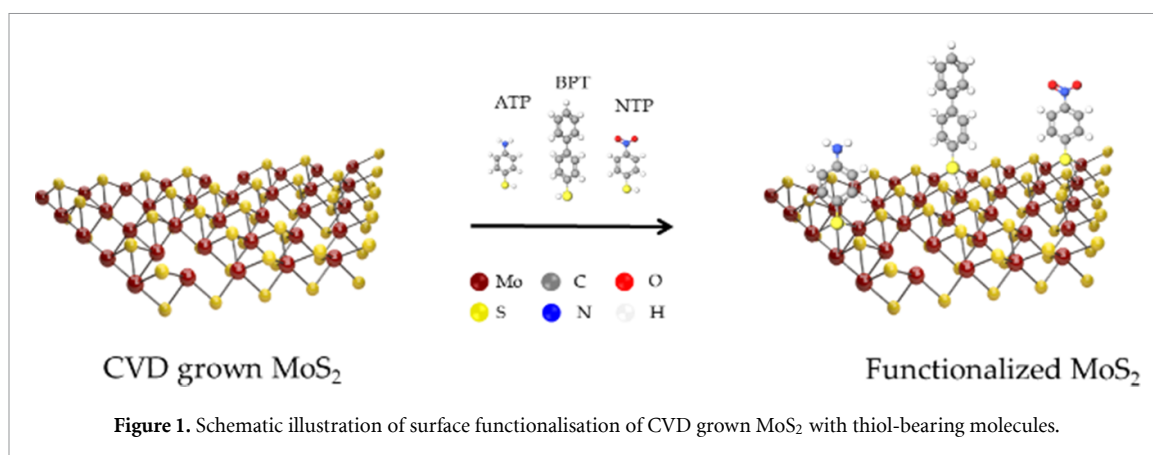*   Author to whom any correspondence should be addressed.

E-mail: p.rudolf@rug.nl

Abstract

Vacancies in atomically thin molybdenum disulphide play an essential role in controlling its optical and electronic properties, which are crucial for applications in sensorics, catalysis or electronics. For this reason, defect engineering employing thiol-terminated molecules is used to heal and/or functionalise defective nanosheets. In this work, chemical vapour deposition-grown MoS₂ with different defect densities was functionalised with three molecules: 4-aminothiophenol (ATP), biphenyl-4-thiol (BPT) and 4-nitrothiophenol (NTP). The molecules' efficacy in functionalising MoS₂ was probed by x-ray photoelectron, Raman and photoluminescence (PL) spectroscopy. The results show that exposing a defective single layer of MoS₂ to either ATP, BPT or NTP molecules heals the defects, however the chemical structure of these molecules affects the optical response and only for BPT the PL intensity increases.

1. Introduction

In recent years, single layer semiconducting transition metal dichalcogenides (TMDs) have attracted massive attention as promising candidates for electronic and optoelectronic devices [1]. The most studied member of this family is single-layer MoS₂, a direct bandgap semiconductor with outstanding physical properties and potential applications in electronic devices [2, 3]. MoS₂ can be produced by mechanical exfoliation using scotch tape [4], by liquid or chemical exfoliation [5, 6] and by chemical vapour deposition (CVD) [7]. The latter approach is the only upscalable method to attain high-quality large domain MoS₂ nanosheets [8, 9]. However, single sulphur vacancies (V_S), single molybdenum vacancies (V_{Mo}) and divacancies (V_{SS}, V_{MoS}) are thermodynamically favoured and always occur during CVD growth [10, 11]. Such undesired defects, as well as grain boundaries and edges decrease the photoluminescence (PL) of single-layer MoS₂. Zhang *et al* [12] established a powerful strategy to heal the sulphur vacancies in single-layer MoS₂ using poly(4-styrenesulfonate) molecule. The self-healing mechanism, where sulphur vacancies are healed spontaneously by sulphur adatom clusters on the MoS₂ surface through a poly(4-styrenesulfonate) (PSS)-induced hydrogenation process, was found to lead to an enhancement of the photoluminescence (PL) intensity. Also sulphur-containing functional molecules can bond to unsaturated Mo edges or sulphur vacancies in MoS₂ surface [13, 14] and thiol chemistry has been exploited to heal and/or functionalise these defect sites with molecules containing an SH group [15, 16]. However, healing of single-layer MoS₂ vacancies does not necessarily bring about an enhancement of the PL intensity but the latter depends on the specific molecule employed [12, 13, 17]. Sim *et al* [13] demonstrated that adsorption of NH₂-containing thiol molecules with lone electron pairs can act as an n-dopant for exfoliated defect-rich single-layer MoS₂, leading to a substantial increase of electron density, and correspondingly to a red-shifted and noticeably weakened PL. Chemisorbed CF₃-terminated thiol molecules provide instead a p-doping effect, resulting in

Figure 1. Schematic illustration of surface functionalisation of CVD grown MoS$_2$ with thiol-bearing molecules.

an increased photoluminescent emission. Ding *et al* [17] also reported a simple approach to covalently functionalise CVD-grown 2H-MoS$_2$ monolayers via thiol conjugation; an enhanced PL response was observed for functionalised MoS$_2$ with 4-fluorobenzyl mercaptan and other thiol-containing molecules. In our previous work, we showed that thiol-terminated cysteine binds covalently to MoS$_2$ to preferentially heal single sulphur vacancies and that it can also fill more complex vacancies [18]. Here we followed the same approach, functionalising CVD-grown single-layer MoS$_2$ with three molecules (see figure 1), namely 4-aminothiophenol (ATP), biphenyl-4-thiol (BPT) and 4-nitrothiophenol (NTP), to understand whether there are differences in the efficacy with which these molecules fill monosulphur vacancies as well as more complex defects, which we created by annealing the as-grown samples to 250 °C. Our attention was on the influence of these adsorbed molecules on the PL of single-layer MoS$_2$ and we specifically investigated whether all three molecules produce an enhancement or a reduction of photoluminescent emission. For this reason, we chose two nitrogen-containing molecules as ATP and NTP, and BPT as nitrogen-free molecule. Our main goal was to demonstrate whether nitrogen-containing molecules always reduce the photoluminescent response of MoS$_2$, as previously suggested [13] and whether defect healing restores the photoluminescent properties also for a more important defect density than that naturally present in CVD-grown single-layer MoS$_2$. Important differences for the three molecules tested were found: grafting BPT on as-grown MoS$_2$ enhanced the photoluminescent response of MoS$_2$, while chemisorbing ATP and NTP resulted in a reduced PL intensity. On the other hand, no improvement in photoluminescent response was found after functionalisation of annealed (and hence defect rich) MoS$_2$ with any of the three molecules. This suggests that the high concentration of molecules on annealed MoS$_2$ is responsible for the reduced PL response after functionalisation with BPT.

2. Methods

2.1. Materials
Pure MoO$_3$ (99.95%) was purchased from Alfa Aesar, sulphur ($\geqslant$99.5%) and BPT with 97% purity were acquired from Sigma Aldrich; ATP with >98.0% purity and NTP with >95.0% purity were bought from Tokyo Chemical Industry. ATP, BPT and NTP were used as received.

2.2. Preparation of monolayer MoS$_2$ by CVD
MoS$_2$ nanosheets were grown in a home-built CVD system with a 60 cm long and 4 cm wide (inner diameter) quartz tube. To achieve optimal temperature control, the quartz tube was surrounded by a Carbolite Gero TF1 single zone furnace, fitted with a Carbolite Gero EPC3016P1 controller and placed where the MoO$_3$ boat and the substrate were located, and a metallic heating belt was placed in correspondence to the sulphur source. Argon (99.999%, Linde) was chosen as the carrier gas, while N-doped silicon (100) wafers with a 300 nm oxide capping (Prime Wafers) were used as substrate. 20 mg MoO$_3$ in a quartz boat and the substrate were positioned in the middle of the furnace, 22 cm away from the S source. The growth protocol comprised four steps: pumping, purging, induction and growth. First, the system was pumped down at room temperature to a pressure of 1.0×10^{-2} mbar; then purging was performed at room temperature by letting argon gas flow at 220 sccm for 10 min; after that the temperature of the furnace surrounding the substrate and the MoO$_3$ boat was increased at 15 °C min^{-1} until it reached 600 °C and left at this temperature for 3 min. Subsequently, the Ar flow rate was decreased to 8 sccm and the furnace temperature augmented at a rate of 2.5 °C min^{-1} to 700 °C. When the chamber reached 610 °C, the heating belt surrounding the sulphur boat was brought to 150 °C to start sulphur sublimation. After 12 min of growth with the furnace around

MoO$_3$ at 700 °C, the furnace was switched off and its temperature left to slowly go down; the flow of Ar was switched off when the temperature reached 350 °C, leaving the sample to cool down to room temperature.

2.3. Annealing procedure and functionalisation of MoS$_2$ by ATP, BPT and NTP

To produce MoS$_2$ with higher defect density [18], we annealed the as-grown MoS$_2$ samples at 250 °C for 1 h under an Ar flow of 300 sccm, using the same CVD setup employed for the growth. The as-grown or annealed MoS$_2$ on Si/SiO$_x$ was immersed in a 0.5 M solution of BPT in chloroform; for ATP a 0.16 M and NTP a 0.13 M solution in ethanol, were used. The samples were kept 48 h in solution, rinsed three times with the respective pure solvent and blown dry with argon.
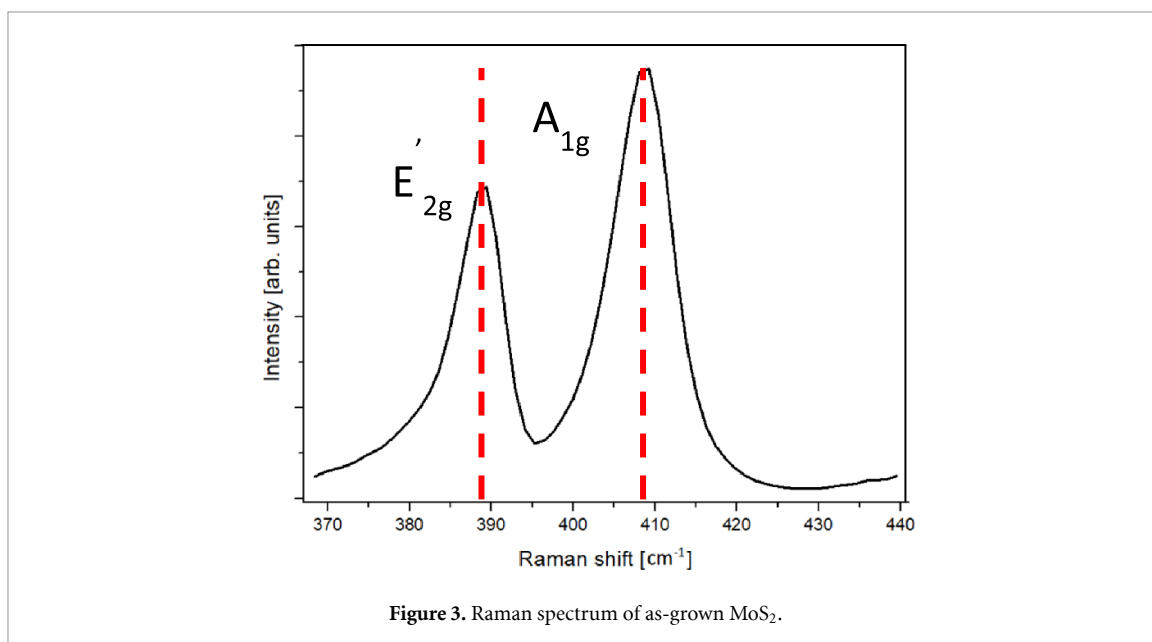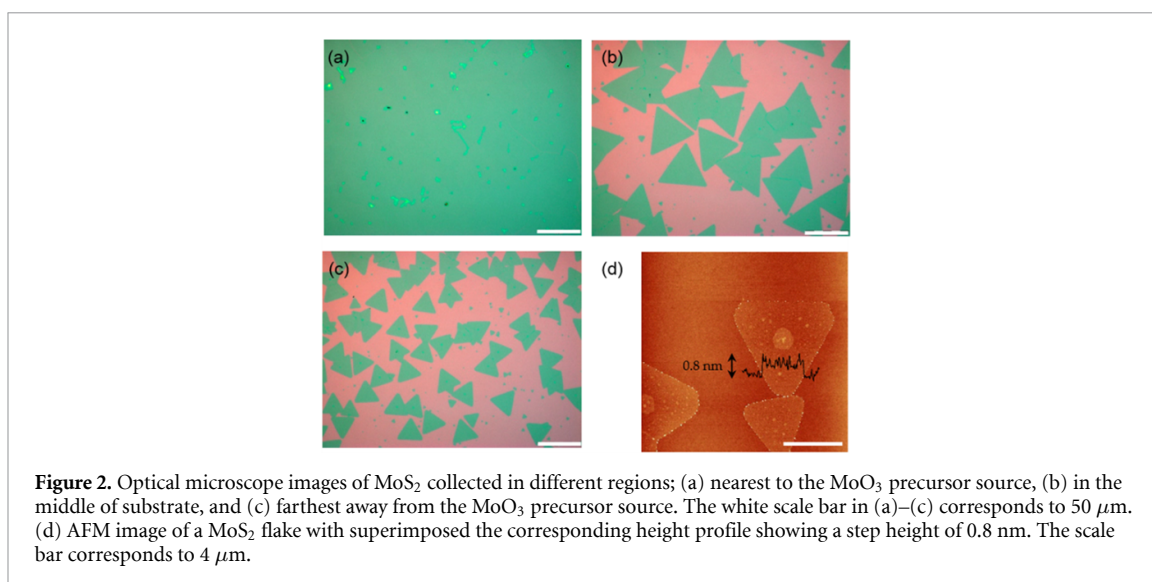
2.4. Sample characterization

Optical microscopy was performed with an Olympus microscope. Atomic force microscopy (AFM) images were recorded in tapping mode with a Scientec 5100, equipped with a silicon cantilever (Budget Sensor) with a resonance frequency of 300 kHz and a force constant of 40 N m^{-1}; the images were analysed using the WSXM program developed by Nanotech [19]. Attenuated total reflection-Fourier transform infrared (ATR-FTIR) spectra recorded on a Bruker VERTEX 70 spectrometer equipped with an ATR diamond single reflection accessory. The measurement resolution was 4 cm^{-1} and the spectra were collected in the range of 4000-400 cm^{-1}, with 32 scans for each sample. Atmospheric compensation and baseline correction were applied to the collected spectra using OPUS spectroscopy software (v7.0) (Bruker Optics). X-ray photoelectron spectroscopy (XPS) data were collected using a Surface Science Instruments SSX-100 ESCA instrument equipped with a monochromatic Al Kα x-ray source (hν = 1486.6 eV). During the measurement, the pressure was kept below 2.0×10^{-9} mbar in the analysis chamber; the electron take-off angle with respect to the surface normal was 37°. The XPS data were acquired using a spot size of 1000 μm in diameter and the energy resolution was set to 1.26 eV for both the survey spectra and the detailed spectra of the Mo3d/S2s, S2p and N1s core level regions. Binding energy values are reported $\pm$0.1 eV and referenced to the Si2p photoemission peak centred at a binding energy of 103.5 eV [20, 21]. All spectra were analysed using the least squares fitting program Winspec (LISE laboratory, University of Namur, Belgium). Deconvolution of the spectra included a Shirley baseline subtraction and fitting with a minimum number of peaks consistent with the structure of the surface, taking into account the experimental resolution. The peak profile was taken as a convolution of Gaussian and Lorentzian functions. The uncertainty in the peak intensity determination was within 2% for the Mo3d/S2s core level region and 3% for the S2p and N1s core level regions. All measurements were carried out on two spots of freshly prepared samples to check for homogeneity. Raman spectra were acquired with a μ-Raman Olympus U-TV1XC microscope, fibre-coupled to an Andor DV420A-BV detector, employing an excitation wavelength of 532 nm. The laser beam size at the sample was about 10 μm in diameter, and the laser power 300 μW. Each spectrum was the average of 20 scans collected with an estimated 0.5 cm^{-1} resolution. The optical microscope with 100 times magnification of the Raman microscope was used. The PL spectra were acquired with an ANDOR SR-500i-D1-R spectrometer, equipped with a 600 lines mm^{-1} grating and coupled to an ANDOR DV420A-OE CCD camera. The laser excitation source had a wavelength of 532 nm, the beam size at the sample was about 10 μm in diameter and the laser power of 0.3 mW. The spectral resolution was 0.5 nm. Each spectrum was recorded with 1 s acquisition time to avoid local overheating by the laser.

3. Results and discussion

An optical microscope was used to visualise the coverage and shape of the MoS$_2$ flakes on the substrate as well as to verify what area of the substrate was completely covered by a continuous film after CVD growth (see figure 2). In figures 2(a)–(c), MoS$_2$ appears green, while the Si/SiO$_x$ substrate is pink. In the region of the substrate closest to the MoO$_3$ precursor during growth, the uniform green contrast gives the first confirmation that a homogeneous film of MoS$_2$ fully covers the substrate (see figure 2(a)). In the regions farthest away from the MoO$_3$ source during growth (figure 2(c)), triangle-shaped islands are distinguished; the islands increase in size and start to merge (figure 2(b)), approaching the region with continuous coverage. Moreover, both on top of the flakes and on the continuous layer, tiny islands indicating the start of second layer growth can be distinguished (brighter spots). The height of a truncated triangular MoS$_2$ flake was determined with the help of AFM, as shown in figure 2(d). As evident from the height profile superimposed on the AFM image, the step height of the MoS$_2$ flake is ∼0.8 nm, which corresponds to the thickness of a single layer [7].

Since the Raman peak positions inform on the thickness of the 2D material [22], Raman spectroscopy was performed on the as-grown MoS$_2$ to confirm the monolayer nature of the flakes. The spectrum in figure 3 shows at 388.8 and 408.7 cm^{-1} the E'$_{2g}$ and A$_{1g}$ Raman active modes corresponding to in-plane and

Figure 2. Optical microscope images of MoS$_2$ collected in different regions; (a) nearest to the MoO$_3$ precursor source, (b) in the middle of substrate, and (c) farthest away from the MoO$_3$ precursor source. The white scale bar in (a)–(c) corresponds to 50 μm. (d) AFM image of a MoS$_2$ flake with superimposed the corresponding height profile showing a step height of 0.8 nm. The scale bar corresponds to 4 μm.

Figure 3. Raman spectrum of as-grown MoS$_2$.

out-of-plane vibrations of MoS$_2$, respectively [9, 23]. The frequency difference of 19.9 cm^{-1} between these modes confirms that MoS$_2$ consists of a single layer [24, 25], in agreement with the AFM results.

To verify the presence of ATP, BPT or NTP on the surface of the sample, Fourier-transform infrared spectroscopy (FTIR) measurements were performed after deposition of the molecules on the as-grown and annealed single-layer MoS$_2$ following the protocol detailed in the experimental section. After functionalisation, the FTIR spectra shown in figure S1 of the supplementary material are the same for all samples and confirm the presence of benzene rings, a common part of the chemical structure of three molecules employed in this study. In particular, the peak at 735–736 cm^{-1} is ascribed to the out-of-plane C–H vibration, while the peaks at 1338–1339 cm^{-1} and 1506–1507 cm^{-1} are attributed to the benzene ring vibration modes [26]. However, due to the low concentration of ATP, BPT or NTP on the surfaces and the correspondingly very low intensity of the bands deriving from NO$_2$ and NH$_2$ vibrations, we cannot detect any distinguishing bands in any of the three spectra of the functionalised surfaces.

Since XPS is a surface sensitive technique for determining the stoichiometry and identifying the type of chemical bonds present, it can reveal whether the different thiol-bearing molecules bind to MoS$_2$. Figure 4(a) shows the photoemission spectra of the Mo3d/S2s core level region of MoS$_2$ before and after functionalisation. All spectra can be deconvoluted with two doublets and one singlet. The main doublet located at a binding energy (B.E.) of 229.8 eV (marked in red in figure 4(a)) represents the contribution of Mo atoms in intrinsic regions (i-Mo^{4+}) of MoS$_2$. In contrast, the doublet at higher B.E. (green) is ascribed to unreacted MoO$_3$ [18, 27]. In all spectra, the singlet located at lower B.E. corresponds to the S2s line of S atoms in defect-free MoS$_2$ [18].
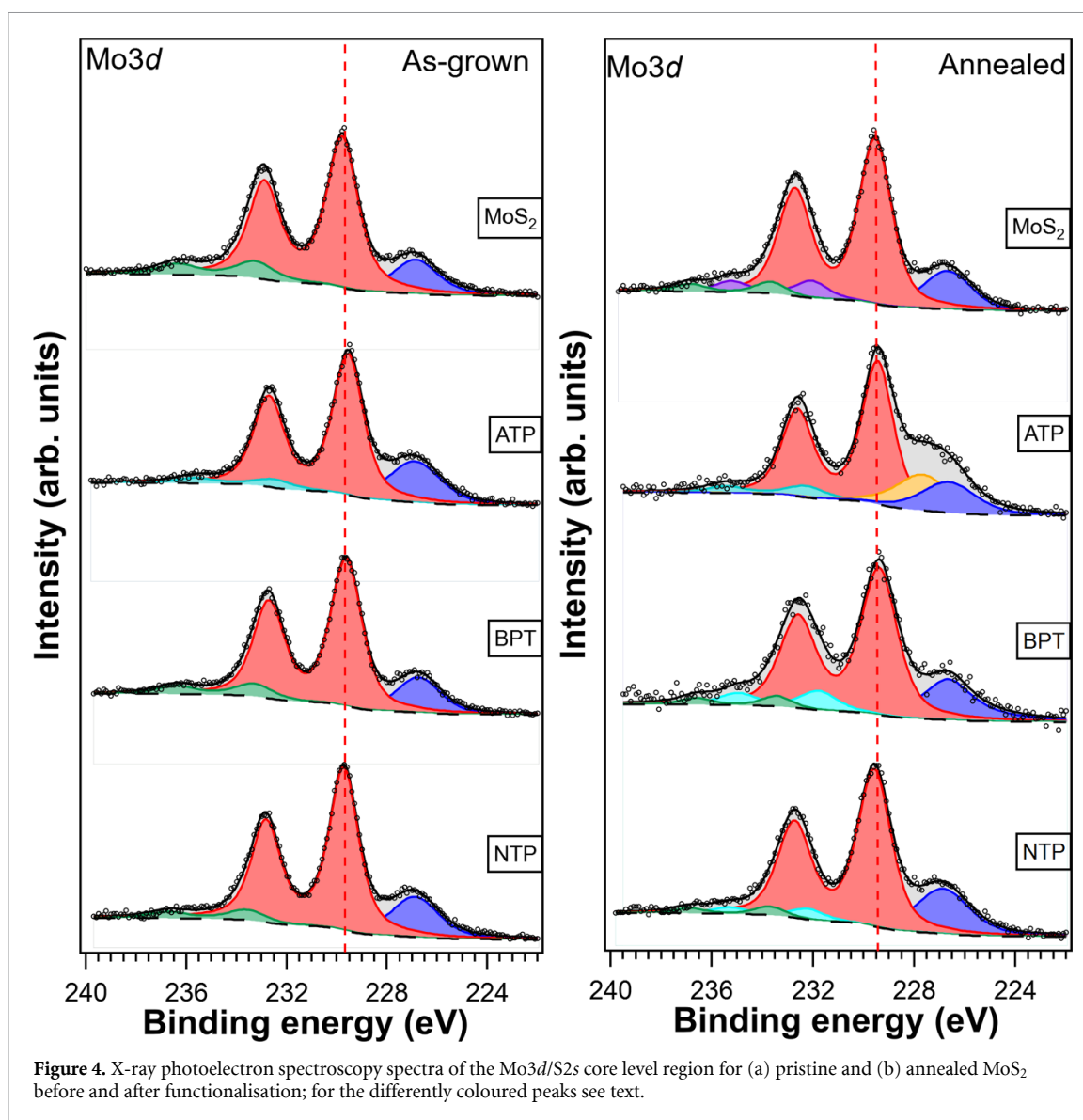
Figure 4. X-ray photoelectron spectroscopy spectra of the Mo3*d*/S2*s* core level region for (a) pristine and (b) annealed MoS$_2$ before and after functionalisation; for the differently coloured peaks see text.

After functionalisation with ATP, the component assigned to the MoO$_3$ precursor residues disappears and a new doublet peaked at a B.E. of 232.4 eV (light blue) appears. The presence of this component, which can be ascribed to MoS$_2$ in a new bonding environment, together with the shift (-0.2 eV) of the main i-Mo^{4+} component, proves the presence of ATP molecules on the surface of the dichalcogenide layer. In the case of grafting BPT or NTP, the MoO$_3$ component is lower in intensity compared to as-grown MoS$_2$ but does not completely disappear as in the spectrum collected after functionalization with ATP. Furthermore, the peak assigned to the presence of the molecules cannot be resolved and the i-Mo^{4+} features are at the same binding energy as for bare MoS$_2$, within the experimental uncertainty. These results show that BPT and NTP are less effective than ATP in functionalising the MoS$_2$ surface. On the other hand, both in the case of NTP and of ATP grafting, the presence of the molecules on the surface is corroborated by the detection of the nitrogen peak (see figure S2(a) in the supplementary material [28]). Furthermore, all S2*p* spectra of the as-grown samples before and after functionalisation can be fitted with one component (see figure S3(a) in the supplementary material) [28]. It is worth noting that unlike in our previous work [18], in the pristine Mo3*d*/S2*s* and S2*p* core level regions, no component assigned to defective MoS$_2$ can be resolved, indicating that the MoS$_2$ of the present study is of better quality. Consequently, despite grafting with ATP molecules being more effective than BPT and NTP, the chemical functionalisation is not so pronounced because of the low number of defects in the as-grown MoS$_2$. We further investigated whether the molecules can also heal vacancies in MoS$_2$. For this, the MoS$_2$ samples were annealed before the functionalisation step to induce sulphur desorption and introduce additional defect sites [18, 29]. Figure 4(b) shows the XPS spectra of the Mo3*d*/S2*s* core level region for the annealed MoS$_2$ before and after the functionalisation. In this case, all the i-Mo^{4+} features (red) are aligned at a B.E. of 229.5 eV, within the experimental uncertainty. Moreover, as already reported in our previous study [18] for annealed MoS$_2$ before grafting, the deconvolution of the

Mo3*d* core level region requires an additional doublet (marked in purple in figure 4(b)) peaked at a B.E. of about 232.0 eV (d-Mo^{4+}). This feature is associated with the presence of defects like sulphur or molybdenum vacancies, which tend to be filled by hydrogen and oxygen from the environment [18].

On the other hand, the Mo3*d*/S2*s* spectrum of annealed MoS$_2$ after grafting ATP (figure 4, right panel) does not show this doublet associated with the presence of defects, confirming the healing of sulphur vacancies; moreover, as in the case of ATP on as-grown MoS$_2$, a doublet at about 232.4 eV (light blue) is detected. The presence of ATP on the surface is also confirmed by the presence of a nitrogen peak (see figure S2(b) in the supplementary material [28]). In addition, a new peak in the S2*s* region appears (orange), located at B.E. of 227.7 eV, which can be tentatively assigned to the formation of S–S bonds, highlighting the possibility that interaction between adsorbed molecules occurs[30].
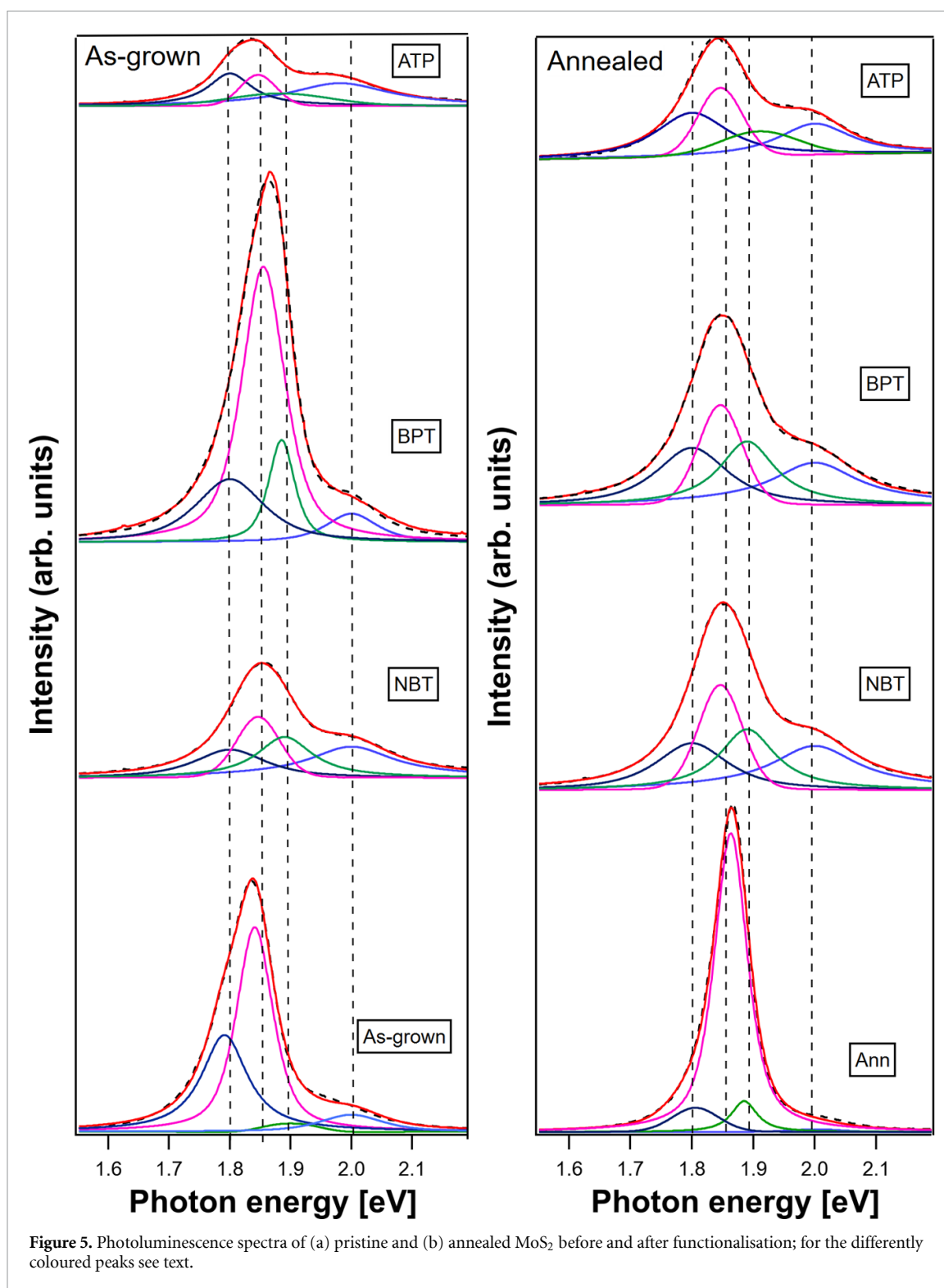
In the Mo3*d*/S2*s* core level spectrum of annealed MoS$_2$ after grafting BPT or NTP the components relative to Mo in defect-free, intrinsic regions (i-Mo^{4+}) of MoS$_2$ (marked in red in figure 3(b)) as well as to MoO$_3$ (green) are observed. Also in this case, the intensity of the MoO$_3$ feature decreased after functionalisation. Additionally, new doublets (light blue) peaked at B.E.s of 231.5 eV for BPT and of 232.2 eV for NTP are required for a good fit; these components are attributed to the molecules adsorbed on MoS$_2$, pointing to healing of sulphur vacancies. Moreover, the presence of NTP on the surface is again evident from the detection of the nitrogen peak (see figure S2(b) in the supplementary material [28]). All S2*p* spectra (see figure S3 (right panel) in the supplementary material [28]) of the annealed samples before and after functionalisation with NTP and BPT were deconvoluted with one component. However, two doublets were needed for the fit of the spectrum collected after grafting with ATP, in agreement with the S2*s* core level region (see figure S3 (right panel) in the supplementary material).

PL measurements were performed to investigate the effect of the chemisorbed molecules on the optical band gap of MoS$_2$ [31, 32] and on the excitonic recombination processes, which are sensitive to the charge carrier density [33, 34]. Figure 5 presents the PL spectra of both as-grown and annealed samples before and after functionalisation; the spectra show an intense peak located at a photon energy of about 1.85 eV and a minor feature at 2.00 eV that can be attributed respectively to the A and B excitons arising from the splitting of the valence band [35, 36]. To gain further insight into the excitonic recombination processes, a deconvolution analysis was carried out by fitting each spectrum with four mixed Gaussian–Lorentzian peaks: the neutral exciton A^0 ($\sim$1.89 eV, green), the negatively charged trion A$^-$ ($\sim$1.85 eV, pink), the B exciton ($\sim$2.00 eV, purple), and the defect-bound exciton D ($\sim$1.80 eV, blue), which can be related to intrinsic structural defects or adsorbates [37]. The as-grown sample is characterized by a strong A$^-$ peak, typical of single-layer MoS$_2$ on SiO$_2$/Si [38]. The presence of an intense trion peak (A$^-$) in fact is related to the excitation power of the laser light employed for the measurements, as explained by Golovynskyi *et al* [39] for experimental condition comparable with ours. Besides this, there is also a strong D peak due to the presence of MoO$_3$ precursor residuals, in agreement with the XPS analysis discussed above, while the contribution of the A^0 and B peaks is almost negligible. In the case of functionalisation with NTP and ATP molecules the healing of the vacancies leads to the increase of the intensity of the A^0 peak and a broadening of the D peak because of the multi-excitonic contribution of the molecules as already reported by Li *et al* [40]. The overall intensity of the PL peak in the case of functionalisation of as-grown MoS$_2$ with nitrogen-containing molecules decreases. ATP and NTP could act as n-dopants for MoS$_2$, similarly to the results reported by Sim *et al* [13] for other nitrogen-containing molecules. After adsorption of BPT, healing of vacancies enhances the A$^-$ peak, resulting in the general increase of PL by 47%, in agreement with the findings of Su *et al* [41] for other nitrogen-free molecules. In the case of the annealed sample, the PL spectrum is still dominated by the A$^-$ contribution, while grafting all three adsorbed molecules enhanced the A^0/A$^-$ ratio. Remarkably, the functionalisation of this defect-rich surface with BPT does not lead to an increase the total PL intensity. This effect is probably due to a larger density of molecules on the sample, which might open non-radiative channels.

To shed further light on the optical response after molecular functionalisation, we also collected PL spectra at 77 K (see figure S4 in the supplementary material [28]). We found for the as-grown single-layer MoS$_2$ that the PL intensity increased by about 30%, while for the functionalised samples the PL intensity decreased. This effect was stronger for functionalised annealed MoS$_2$ samples that have a higher coverage of molecules. However, for both the functionalised as-grown and annealed MoS$_2$ the intensities of the PL spectra were restored when we warmed them up to room temperature. This behaviour points to a structural rearrangement of the adsorbed molecules at low temperature, which opens non-radiative channels and hence partially quenches PL.

Our functionalization method differs from others reported in the literature [42, 43] where the covalent bonding of molecules goes hand in hand with a phase transition from 2H-MoS$_2$ to 1T-MoS$_2$, which is metallic. In our case, the single-layer MoS$_2$ keeps its semiconducting nature, as demonstrated by the PL measurements. In addition, with respect to our previous work [18], where we showed with a similar

Figure 5. Photoluminescence spectra of (a) pristine and (b) annealed MoS_2 before and after functionalisation; for the differently coloured peaks see text.

approach employing cysteine that the adsorbed molecules were not able to completely heal the defects, in this case the XPS peak related to defect sites completely disappeared after functionalisation.

4. Conclusions

In conclusion, we examined the different behaviour of thiol-bearing molecules on MoS_2, revealing that adsorption of these molecules led to healing of S vacancies inherent to CVD growth. XPS analysis of the as-grown MoS_2 showed that ATP chemisorbed to the dichalcogenide layer and the MoO_3 precursor residues were eliminated when functionalising the sample. Conversely, the adsorption of BPT or NTP only slightly affected the chemical properties of the single-layer MoS_2, and the presence of a different chemical state could

not be resolved. Furthermore, when additional sulphur vacancies were created by annealing the MoS_2 surface. XPS analysis gave evidence for the disappearance of the spectroscopic fingerprint associated with defects after exposing the samples to either ATP, BPT or NTP, demonstrating the ability of these molecules to heal defects also in this case. In particular, we proved that the nitrogen-containing molecules we chose, i.e. ATP and NTP, reduced the photoluminescent response of as-grown MoS_2, highlighting that they acted as n-dopants. Conversely, functionalisation with BPT, a nitrogen-free compound, led to an enhancement of the PL intensity for the as-grown MoS_2. After annealing of MoS_2, no improvement in PL intensity was found after functionalisation with either of the three molecules, i.e. BPT adsorption was not beneficial in this case. The high concentration of molecules on the annealed MoS_2 could play a critical role on the reduced PL response after functionalisation with BPT.

Data availability statement

All data that support the findings of this study are included within the article (and any supplementary files).

Acknowledgments

Author contributions

P R, O D L, A S conceptualisation; G F, O D L, investigation, formal analysis, validation, visualisation; S H, A A E Y investigation; G F, O D L, P R writing the original draft; P R, R G A, O D L, J Y supervision; all authors reviewed and edited the manuscript and the supporting material.

Conflict of interest

There are no conflicts to declare.

ORCID iDs

Giovanna Feraco ⬤ https://orcid.org/0000-0001-8008-5283
Oreste De Luca ⬤ https://orcid.org/0000-0002-4428-0863
Ali Syari'ati ⬤ https://orcid.org/0000-0003-0161-8980
Sardar Hameed ⬤ https://orcid.org/0000-0002-2312-8440
Abdurrahman Ali El Yumin ⬤ https://orcid.org/0000-0002-2509-0669
Jianting Ye ⬤ https://orcid.org/0000-0002-3667-3069
Raffaele G Agostino ⬤ https://orcid.org/0000-0002-5172-1866
Petra Rudolf ⬤ https://orcid.org/0000-0002-4418-1769

References

[1] Radisavljevic B, Radenovic A, Brivio J, Giacometti V and Kis A 2011 Single-layer MoS_2 transistors *Nat. Nanotechnol.* **6** 147–50
[2] Yin L, Cheng R, Wen Y, Liu C and He J 2021 Emerging 2D memory devices for in-memory computing *Adv. Mater.* **33** e2007081
[3] Migliato Marega G, Zhao Y, Avsar A, Wang Z, Tripathi M, Radenovic A and Kis A 2020 Logic-in-memory based on an atomically thin semiconductor *Nature* **587** 72–77
[4] Mak K F, Lee C, Hone J, Shan J and Heinz T F 2010 Atomically thin MoS_2: a new direct-gap semiconductor *Phys. Rev. Lett.* **105** 136805
[5] Varrla E, Backes C, Paton K R, Harvey A, Gholamvand Z, McCauley J and Coleman J N 2015 Large-scale production of size-controlled MoS_2 nanosheets by shear exfoliation *Chem. Mater.* **27** 1129–39
[6] Eda G, Fanchini G and Chhowalla M 2008 Large-area ultrathin films of reduced graphene oxide as a transparent and flexible electronic material *Nat. Nanotechnol.* **3** 270–4
[7] Zhan Y, Liu Z, Najmaei S, Ajayan P M and Lou J 2012 Large-area vapor-phase growth and characterization of MoS_2 atomic layers on a SiO_2 substrate *Small* **8** 966–71
[8] Lee Y H *et al* 2012 Synthesis of large-area MoS_2 atomic layers with chemical vapor deposition *Adv. Mater.* **24** 2320–5
[9] Kim Y, Bark H, Ryu G H, Lee Z and Lee C 2016 Wafer-scale monolayer MoS_2 grown by chemical vapor deposition using a reaction of MoO_3 and H_2S *J. Phys.: Condens. Matter* **28** 184002
[10] Zhou W, Zou X, Najmaei S, Liu Z, Shi Y, Kong J, Lou J, Ajayan P M, Yakobson B I and Idrobo J C 2013 Intrinsic structural defects in monolayer molybdenum disulfide *Nano Lett.* **13** 2615–22
[11] Haldar S, Vovusha H, Yadav M K, Eriksson O and Sanyal B 2015 Systematic study of structural, electronic, and optical properties of atomic-scale defects in the two-dimensional transition metal dichalcogenides MX^2 (M = Mo, W; X = S, Se, Te) *Phys. Rev.* B **92** 235408

[12] Zhang X *et al* 2017 Poly(4-styrenesulfonate)-induced sulfur vacancy self-healing strategy for monolayer MoS$_2$ homojunction photodiode *Nat. Commun.* **8** 15881

[13] Sim D M, Kim M, Yim S, Choi M-J, Choi J, Yoo S and Jung Y S 2015 Controlled doping of vacancy-containing few-layer MoS$_2$ via highly stable thiol-based molecular chemisorption *ACS Nano* **9** 12115–23

[14] Lauritsen J V, Nyberg M, Vang R T, Bollinger M V, Clausen B S, Topsøe H, Jacobsen K W, Lægsgaard E, Nørskov J K and Besenbacher F 2003 Chemistry of one-dimensional metallic edge states in MoS$_2$ nanoclusters *Nanotechnology* **14** 385

[15] Chen X, Berner N C, Backes C, Duesberg G S and McDonald A R 2016 Functionalization of two-dimensional MoS$_2$: on the reaction between MoS$_2$ and organic thiols *Angew. Chem., Int. Ed. Engl.* **55** 5803–8

[16] Forster A, Gemming S and Seifert G 2018 Functional thiols as repair and doping agents of defective MoS$_2$ monolayers *J. Phys.: Condens. Matter* **30** 235302

[17] Ding Q, Czech K J, Zhao Y, Zhai J, Hamers R J, Wright J C and Jin S 2017 Basal-plane ligand functionalization on semiconducting 2H-MoS$_2$ monolayers *ACS Appl. Mater. Interfaces* **9** 12734–42

[18] Syari'ati A, Kumar S, Zahid A, Ali El Yumin A, Ye J and Rudolf P 2019 Photoemission spectroscopy study of structural defects in molybdenum disulfide (MoS$_2$) grown by chemical vapor deposition (CVD) *Chem. Commun.* **55** 10384–7

[19] Horcas I, Fernandez R, Gomez-Rodriguez J M, Colchero J, Gomez-Herrero J and Baro A M 2007 WSXM: a software for scanning probe microscopy and a tool for nanotechnology *Rev. Sci. Instrum.* **78** 013705

[20] John F M and Jill Chastain R C K Jr (eds) 1995 *Handbook of X-Ray Photoelectron Spectroscopy: A Reference Book of Standard Spectra for Identification and Interpretation of XPS Data* (Eden Prairie, MN: Physical Electronics)

[21] Mazzoldi P, Carnera A, Caccavale F, Favaro M L, Boscolo-Boscoletto A, Granozzi G, Bertoncello R and Battaglin G 1991 N and Ar ion-implantation effects in SiO$_2$ films on Si single-crystal substrates *J. Appl. Phys.* **70** 3528–36

[22] Kai-Ge Zhou F W, Cao Y, Sheng H, Geliang Y and Casiraghi C 2014 Raman modes of MoS$_2$ used as fingerprint of van der Waals interactions in 2D crystal-based heterostructures *ACS Nano* **8** 9914–24

[23] Deokar G, Vignaud D, Arenal R, Louette P and Colomer J F 2016 Synthesis and characterization of MoS$_2$ nanosheets *Nanotechnology* **27** 075604

[24] Zhang J *et al* 2014 Scalable growth of high-quality polycrystalline MoS$_2$ monolayers on SiO$_2$ with tunable grain sizes *ACS Nano* **8** 6024–30

[25] Tu Z, Li G, Ni X, Meng L, Bai S, Chen X, Lou J and Qin Y 2016 Synthesis of large monolayer single crystal MoS$_2$ nanosheets with uniform size through a double-tube technology *Appl. Phys. Lett.* **109** 223101

[26] Smith B C 2016 Group wavenumbers and an introduction to the spectroscopy of benzene rings *Spectroscopy* **31** 3

[27] Jeon J, Jang S K, Jeon S M, Yoo G, Jang Y H, Park J H and Lee S 2015 Layer-controlled CVD growth of large-area two-dimensional MoS$_2$ films *Nanoscale* **7** 1688–95

[28] See the supplementary material of this article

[29] Donarelli M, Bisti F, Perrozzi F and Ottaviano L 2013 Tunable sulfur desorption in exfoliated MoS$_2$ by means of thermal annealing in ultra-high vacuum *Chem. Phys. Lett.* **588** 198–202

[30] Abdul Razzaq A, Yao Y, Shah R, Qi P, Miao L, Chen M, Zhao X, Peng Y and Deng Z 2019 High-performance lithium sulfur batteries enabled by a synergy between sulfur and carbon nanotubes *Energy Storage Mater.* **16** 194–202

[31] Cheiwchanchamnangij T and Lambrecht W R L 2012 Quasiparticle band structure calculation of monolayer, bilayer, and bulk MoS$_2$ *Phys. Rev.* B **85** 205302

[32] Mak K F and Shan J 2016 Photonics and optoelectronics of 2D semiconductor transition metal dichalcogenides *Nat. Photon.* **10** 216–26

[33] Birmingham B, Yuan J, Filez M, Fu D, Hu J, Lou J, Scully M O, Weckhuysen B M and Zhang Z 2019 Probing the effect of chemical dopant phase on photoluminescence of monolayer MoS$_2$ using *in situ* Raman microspectroscopy *J. Phys. Chem.* C **123** 15738–43

[34] M. H, Han G H, Kim H, Bae J J, Jeong M S and Lee Y H 2016 Photochemical reaction in monolayer MoS$_2$ via correlated photoluminescence, Raman spectroscopy, and atomic force microscopy *ACS Nano* **10** 5230–6

[35] Plechinger G, Mann J, Preciado E, Barroso D, Nguyen A, Eroms J, Schüller C, Bartels L and Korn T 2014 A direct comparison of CVD-grown and exfoliated MoS$_2$ using optical spectroscopy *Semicond. Sci. Technol.* **29** 064008

[36] Yore A E, Smithe K K H, Crumrine W, Miller A, Tuck J A, Redd B, Pop E, Wang B and Newaz A K M 2016 Visualization of defect-induced excitonic properties of the edges and grain boundaries in synthesized monolayer molybdenum disulfide *J. Phys. Chem.* C **120** 24080–7

[37] Su W, Kumar N, Spencer S J, Dai N and Roy D 2015 Transforming bilayer MoS$_2$ into single-layer with strong photoluminescence using UV-ozone oxidation *Nano Res.* **8** 3878–86

[38] Li H, Wu J, Yin Z and Zhang H 2014 Preparation and applications of mechanically exfoliated single-layer and multilayer MoS$_2$ and WSe$_2$ nanosheets *Acc. Chem. Res.* **47** 1067–75

[39] Golovynskyi S, Datsenko O I, Dong D, Lin Y, Irfan I, Li B, Lin D and Qu J 2021 Trion binding energy variation on photoluminescence excitation energy and power during direct to indirect bandgap crossover in monolayer and few-layer MoS$_2$ *J. Phys. Chem.* C **125** 17806–19

[40] Li Y *et al* 2017 Controlled gas molecules doping of monolayer MoS$_2$ via atomic-layer-deposited Al$_2$O$_3$ films *ACS Appl. Mater. Interfaces* **9** 27402–8

[41] Su W, Dou H, Huo D, Dai N and Yang L 2015 Enhancing photoluminescence of trion in single-layer MoS$_2$ using p-type aromatic molecules *Chem. Phys. Lett.* **635** 40–44

[42] Presolski S and Pumera M 2016 Covalent functionalization of MoS$_2$ *Mater. Today* **19** 140–5

[43] Voiry D, Goswami A, Kappera R, e Silva Cde C, Kaplan D, Fujita T, Chen M, Asefa T and Chhowalla M 2015 Covalent functionalization of monolayered transition metal dichalcogenides by phase engineering *Nat. Chem.* **7** 45–49